An overview of the ZTEM and AirMt airborne electromagnetic systems: a case study from the Nebo–Babel Ni–Cu–PGE deposit, West Musgrave, Western Australia

Jean Legault

Jean Legault[1,5], Glenn A. Wilson[2], Alexander V. Gribenko[2,3], Michael S. Zhdanov[2,3], Shengkai Zhao[1] and Keith Fisk[4]

[1]*Geotech, Aurora, Ontario, Canada*
[2]*TechnoImaging, Salt Lake City, Utah, USA*
[3]*The University of Utah, Salt Lake City, Utah, USA*
[4]*Geotech Airborne, Malaga, WA, Australia*
[5]*Corresponding author. Email: jean@geotech.ca*

To improve mineral exploration success, there is an industry-wide consensus on the need to increase the 'discovery space' by exploring under cover and to greater depths. Over the last decade, airborne electromagnetic (AEM) systems have evolved with ever higher moments, and sensor calibration and post-acquisition processing technologies have improved data quality significantly. As an alternative to conventional AEM, the Z-axis Tipper Electromagnetic (ZTEM) and Airborne Magnetic Tensor (AirMt) systems were developed to measure the transfer functions of audio-frequency natural electromagnetic sources from airborne platforms. The ZTEM system measures tipper transfer functions, and the AirMt system measures the rotational invariant of the transfer functions. Ancillary data measured by both systems include radar altimeter, receiver altitude, GPS elevation, and total magnetic intensity. For both ZTEM and AirMt, data are typically measured from 30 Hz to 720 Hz, giving detection depths to 1 km or more, depending on the terrain conductivity. This makes it a practical method for mapping large-scale geological structures. This paper discusses technical specifications of both the ZTEM and AirMt systems, including data processing and interpretation.

Both ZTEM and AirMt capitalise on Geotech's logistical and technical experience from its helicopter-borne Versatile Time-domain ElectroMagnetic (VTEM) system, which has been in commercial operation since 2002 with subsequent generational improvements. The first commercial surveys for ZTEM were commissioned in 2006, and the first commercial surveys for AirMt were commissioned in 2009. Presently, eight ZTEM systems and one AirMt system are in functional operation around the world. ZTEM and AirMt surveys have been flown in Australia, North America, South America, Africa and the Middle East for Sedex, VMS, IOCG, Ni–Cu–PGE, porphyry, uranium and precious metal mineralisation systems for numerous major and junior exploration companies. In this paper, we present a case study for the 3D interpretation ZTEM and AirMt surveys flown over the Nebo–Babel Ni–Cu–PGE deposit in Western Australia.

Background

Since the 1950s, magnetotelluric (MT) surveys have measured horizontal electric and magnetic fields induced from natural sources, which may be treated as plane electromagnetic waves. However, the amplitude and phase of the primary field is unknown. By processing the electric and magnetic fields to a complex impedance tensor, the unknown source terms are removed and the transfer functions are dependent on frequency and the earth's conductivity. Magnetovariational (MV) methods are an extension of the MT concept, whereby the transfer functions between the horizontal and vertical magnetic fields:

$$H_z(r) = W_{zx}(r)H_x(r) + W_{zy}(r)H_y(r),$$

form a complex vector often called the *Weiss–Parkinson vector*, *induction vector*, or *tipper*. Similar to the impedance tensor for MT data, the tipper effectively removes otherwise unknown source terms. Since the vertical magnetic field is zero for plane waves vertically propagating into a 1D earth model, non-zero vertical magnetic fields are directly related to 2D or 3D structures.

This served as the basis for the original development of the audio-frequency magnetic (AFMAG) method (Ward, 1959) whereby two orthogonal coils were towed behind an airborne platform to determine the tilt angle of the plane of polarisation of natural magnetic fields in the 1 Hz to 20 kHz band. The natural magnetic fields of interest originate from atmospheric thunderstorm activity and propagate over large distances with little attenuation in the earth-ionosphere wave guide. Given the
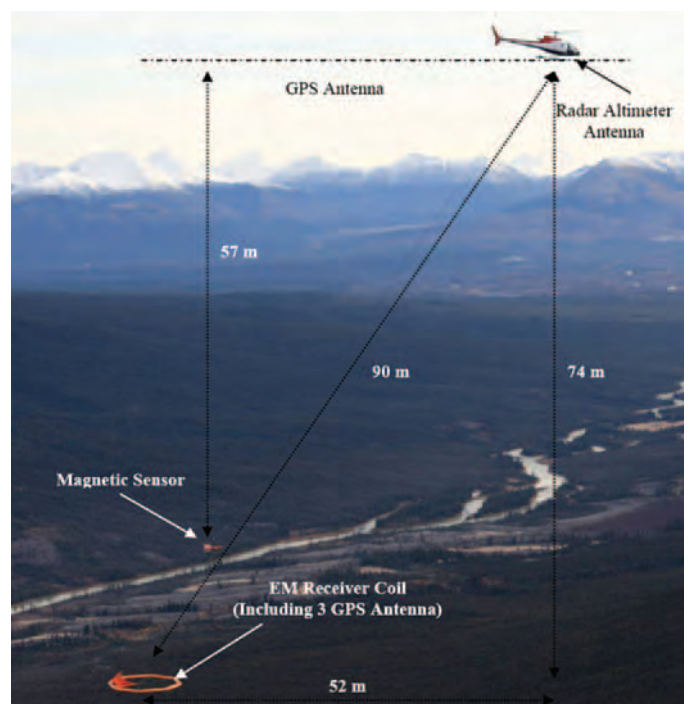

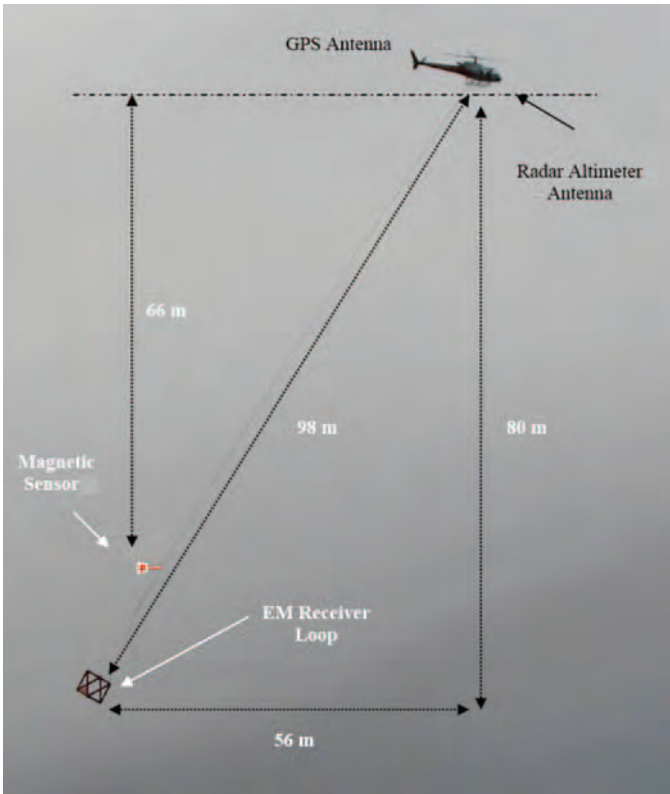**Fig. 1.** *ZTEM (Z-Axis Tipper ElectroMagnetic) system configuration.*

Fig. 2. *AirMt (Airborne Magnetic Tensor) system configuration.*

tilt angle is zero over a 1D earth, the AFMAG method was effective when crossing conductors. However, the direction and amplitude of the natural magnetic fields randomly varies with time and periodically with season, meaning AFMAG data were not repeatable (Ward *et al.*, 1966). By using MT processing techniques for ground-based orthogonal horizontal magnetic field measurements, Labson *et al.* (1985) demonstrated that repeatable tipper data could be recovered from measured magnetic fields.

The AFMAG method of Labson *et al.* (1985) remained largely undeveloped until the recent commercialisation of ZTEM (e.g. Pare and Legault, 2010) (Figure 1) and subsequently, AirMt (e.g. Kaminski *et al.*, 2010) (Figure 2) systems by Geotech. ZTEM measures the tipper components as the transfer function of a vertical magnetic field measured from an airborne receiver (r) to the horizontal components measured at a ground-based reference receiver (r$_0$):

$$H_z(r) = W_{zx}(r, r_0)\, H_x(r_0) + W_{zy}(r, r_0) H_y(r_0),$$

AirMt directly measures the rotational invariant of the transfer function for the three magnetic fields measured from an airborne receiver to the three magnetic fields measured at a ground-based (reference) location. Generalising the Weiss–Parkinson relationship, the three components of a magnetic field measured at a receiver (r) are linearly related to the horizontal magnetic fields measured at a ground-based reference receiver (r$_0$):

$$\begin{bmatrix} H_x(r) \\ H_y(r) \\ H_z(r) \end{bmatrix} = \begin{bmatrix} H_{xx}(r, r_0) & H_{xy}(r, r_0) \\ H_{yx}(r, r_0) & H_{yy}(r, r_0) \\ H_{zx}(r, r_0) & H_{zy}(r, r_0) \end{bmatrix} \begin{bmatrix} H_x(r_0) \\ H_y(r_0) \end{bmatrix},$$

If we write W$_1$ and W$_2$ as the first and second columns of the transfer function, then we can introduce the variable:

$$K = W_1 \times W_2,$$

and obtain the complex scalar:

$$K = K \cdot \frac{Re(K)}{|Re(K)|},$$

called the *amplification parameter* (AP), which can be shown to be rotationally invariant. (Kuzmin *et al.*, 2010; D. J. Dodds, pers. comm., 2010; P. E. Wannamaker, pers. comm., 2010). Since the amplification parameter does not depend on the orientation of the sensor, it negates the post-acquisition need to correct for sensor orientation.

For both ZTEM and AirMt systems, the time series of the magnetic fields are recorded at fixed sampling rates and the data are binned and processed to generate in-phase and quadrature transfer functions in the frequency domain (i.e. tippers for ZTEM; amplification parameter for AirMt). The lowest frequency of the transfer functions depends on the speed of the airborne platform, and the highest frequency depends on the sampling rate. For helicopter-borne or fixed-wing ZTEM and helicopter AirMt systems, transfer functions are typically obtained at five or six frequencies from 20 Hz to 800 Hz, giving skin depths ranging between 600 m and 2000 m for typical terrain conductivities.

Instrumentation

For helicopter surveys, the ZTEM and AirMt systems are carried as an external sling load, and are independent of the helicopter. The ZTEM receiver measured the vertical magnetic field from a 7.4 m diameter air-core loop sensor. The AirMt receiver measures three components of the magnetic field using three mutually perpendicular, 3.04 m diameter air-core loops. Both ZTEM and AirMt receivers are encased in a fibreglass shell that is isolated from most vibrations by a patented suspension system. The receivers are nominally towed from the helicopter by a 90 m long cable, and are flown with a nominal ground clearance of 80 m. Altitude positioning of the receiver is enabled by GPS antennas mounted on the frame. For both ZTEM and AirMt, the magnetic fields are measured with a 2 kHz sampling frequency. The fixed-wing ZTEM (FW-ZTEM) system is currently deployed from a Cessna Grand Caravan. The FW-

Fig. 3. *ZTEM and AirMt base station sensor.*

ZTEM receiver is a 12 m^2 rectangular loop sensor nominally towed 60 m behind and 80 m below the aircraft. Altitude positioning of the receiver is enabled by attitude sensors and GPS antenna mounted on the frame. The magnetic fields are measured with a 2 kHz sampling frequency. The ZTEM payload is sufficiently light that gravimeters and spectrometers can be simultaneously deployed. The base station for these systems is typically the AirMt sensor, consisting of three mutually perpendicular, 3.04 m diameter air-core loops, as shown in Figure 3. The base station provides a reference field, which when processed with the airborne receiver data produces the appropriate transfer functions.

Interpretation

Given the same plane wave source terms, modelling and inversion for ZTEM and AirMt data is similar to that of MT. However, unlike MT surveys, ZTEM and AirMt surveys typically contain hundreds to thousands of line kilometres of data with measurement locations every few metres, covering areas thousands of square kilometres in size. To be practical, the capacity must exist to generate 3D interpretative products with sufficient resolution in sufficient time so as to affect exploration decisions. Geotech's standard products for ZTEM and AirMt include total divergence and phase rotation grids, and 2D Gauss-Newton inversion based on modifications to algorithms by Wannamaker *et al.* (1987), de Lugao and Wannamaker (1996), and Tarantola (1987). Third parties provide additional products such as 2D pseudo-sections by Karous-Hjelt filters (e.g. Sattel *et al.*, 2010) or 2D Occam inversions based on their own modifications of algorithms by Constable *et al.* (1987) and Wannamaker *et al.* (1987). Holtham and Oldenburg (2010) introduced 3D ZTEM inversion based on modifications of the 3D MT inversion by Farquharson *et al.* (2002). In the subsequent case study for both ZTEM and AirMt, our 3D MT inversion analog is that of Zhdanov *et al.* (2011).

Case study: Nebo–Babel Ni–Cu–PGE deposits

Most world-class deposits of nickel and platinum-group elements (PGE) are found in mafic igneous rocks of Proterozoic age and as part of exceptional large igneous provinces (LIPs). The West Musgrave Block, located in central Australia, is one such example but where most of the prospective grounds are beneath regolith. In previous years, access for explorers was difficult due to restrictions imposed by the traditional landholders. Recently,
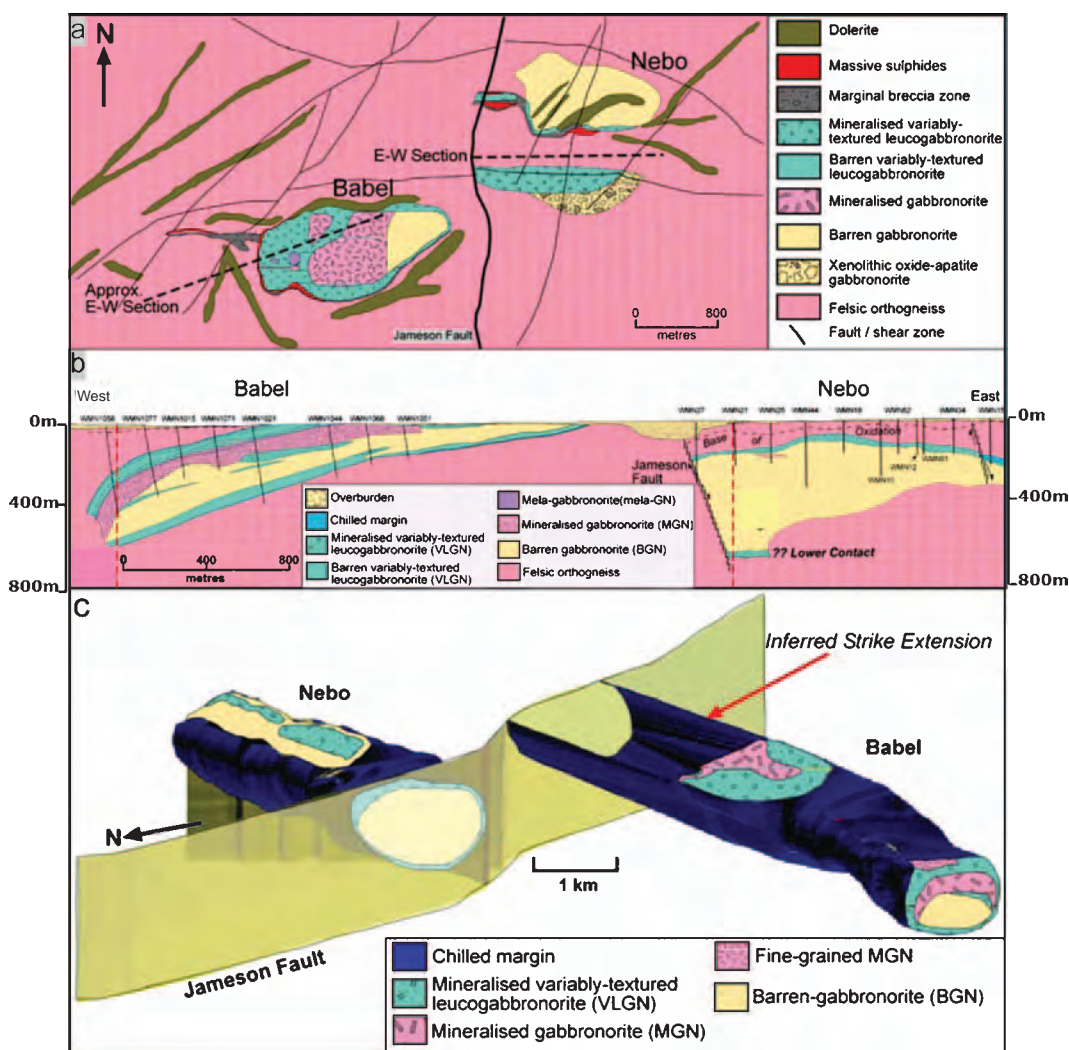

Fig. 4. *(a) Surface projection of the gabbro-norite rock units, mineralised domains, and major structural elements at West Musgrave, (b) longitudinal east-west section though the Nebo–Babel intrusion, (c) south-east facing 3D geological model showing spatial and morphological relationships between the Nebo and Babel parts of the intrusion (after Seat,* et al.*, 2007).*

access has improved with structured agreements between explorers and well organised land councils (Groves *et al.*, 2007). One example of early success in the area was WMC's (now BHP Billiton) surface geochemistry-led discovery of the Nebo–Babel Ni–Cu–PGE deposit in 2000. Nebo–Babel has a number of features in common with other Ni–Cu–PGE deposits hosted in dynamic magma conduits (e.g. Voisey's Bay, Canada), such as multiple magma pulses and sulphide entrainment from depth, rather than *in situ* sulphide segregation (Seat *et al.*, 2007, 2009). Drill intersections include 106.5 m at 2.4% Ni, 2.7% Cu, and 0.2 g/t PGE; and a resource of approximately 1 million tonnes contained Ni and 1 million tonnes contained Cu+Co has been released.

Geology

The Nebo–Babel deposit is hosted within a concentrically zoned, tube-like gabbronorite intrusion (1078 Ma) that has a 5 km east-west extent, a 1 km × 0.5 km cross-section, and a shallow WSW-plunge (Figure 4). The gabbro-norite has intruded felsic orthogneissic country rocks of amphibolite to granulite facies metamorphic grade and is offset along the north-southerly Jameson Fault, which separates the Babel and Nebo deposits that are of similar morphology. Babel is a large, generally EW to SW striking, mainly low-grade disseminated deposit that subcrops through thin sand cover to the east but plunges under more than 400 m of country rock and remains open to a depth of 600 m. Nebo, 2 km to the northeast, is buried under a few metres of aeolian dune sand and is smaller than Babel, but contains a number of high grade massive sulphide pods that are mainly found in the upper part of the intrusion. It extends at least 1.8 km east-west but its eastern limit and lower intrusive contact (inferred at >600 m) have not yet been drill defined. The deposits were discovered using deflation lag sampling on a 1 km × 0.5 km grid drill pattern. However, strong magnetic, electromagnetic, and gravity anomalies highlight the massive and disseminated mineralisation in the deposit. For example, Figure 5 shows the late channel B-field time constant from a GEOTEM survey over the area.
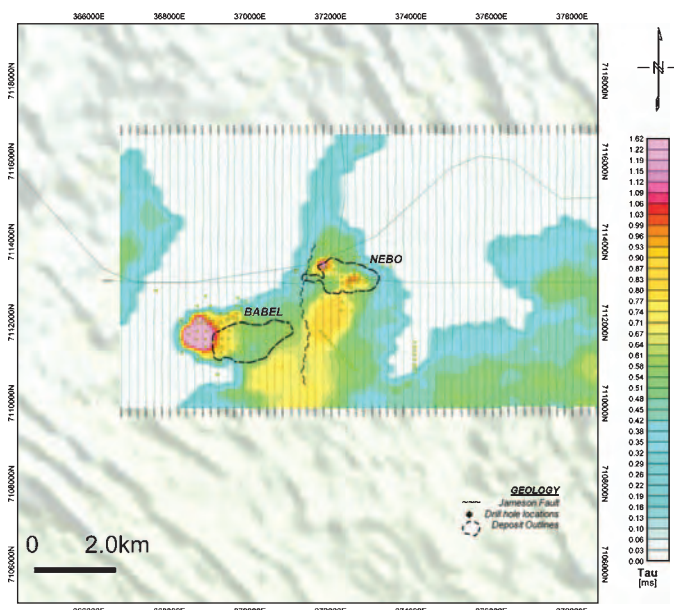
ZTEM and AirMt surveys

Under agreement between Geotech Airborne and BHP Billiton, both ZTEM and AirMt surveys were flown over the Nebo–Babel deposits (Figure 6). A total of 541 line km of ZTEM data and 574 line km of AirMt data were acquired along both east-west and north-south flight lines. The survey area has minimal topographic relief, varying from 460 to 494 m above sea level. The ZTEM receiver was flown with a nominal ground clearance of 78 m. ZTEM data were acquired at six frequencies; 25 Hz, 37 Hz, 75 Hz, 150 Hz, 300 Hz, and 600 Hz. The AirMt receiver was flown with a nominal ground clearance of 78 m. AirMt data were acquired at six frequencies: 24 Hz, 38 Hz, 75 Hz, 150 Hz,
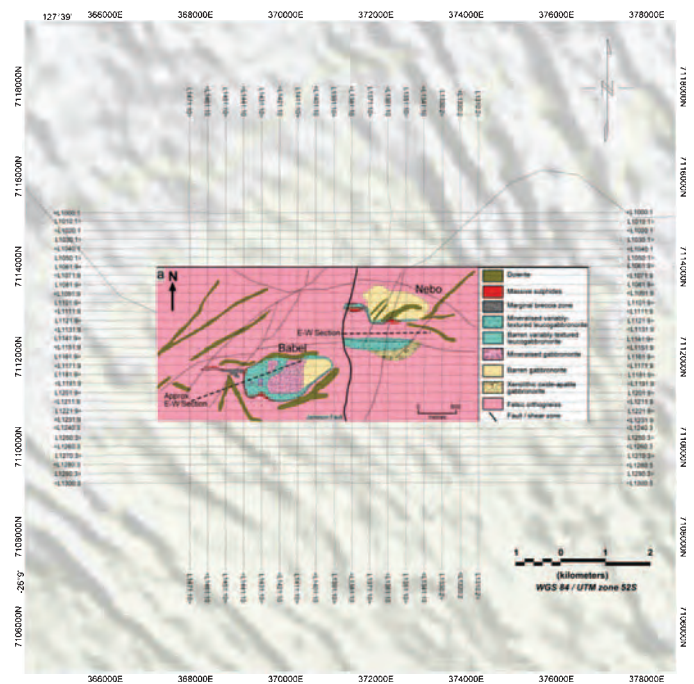

Fig. 6. *ZTEM and AirMt flight lines over Nebo–Babel geology (modified after Seat* et al., *2007).*
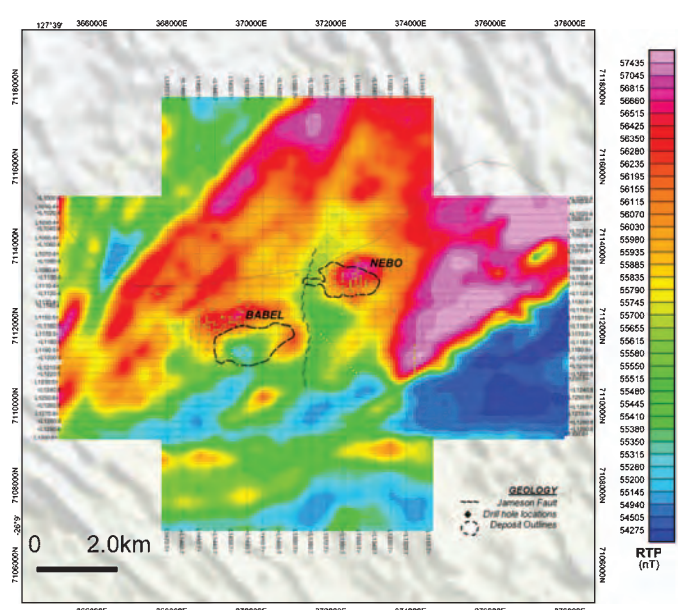

Fig. 5. *GEOTEM late channel B-field time constant.*

Fig. 7. *Total magnetic intensity (TMI) – reduced to pole (RTP).*
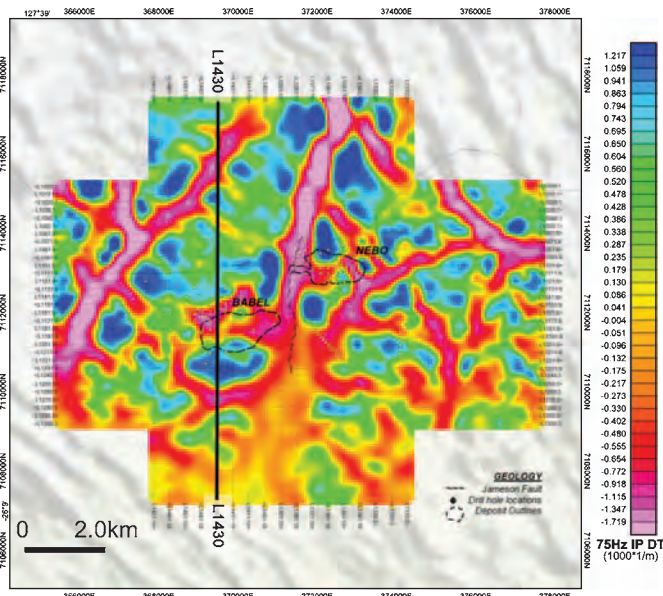
Fig. 8. *ZTEM 75Hz In-Phase Total Divergence (DT).*

image and to compensate for the cross-over nature of ZTEM data, the total divergence (DT) is introduced as the horizontal derivatives of the tipper components:

$$DT = \frac{\partial T_{zx}}{\partial_x} + \frac{\partial T_{zy}}{\partial_y},$$

and is derived for each of the in-phase and quadrature components at individual frequencies. These in turn allow for minima over conductors and maxima over resistive zones. DT grids for each of the extracted frequencies were generated accordingly, using a reverse colour scheme with warm colours over conductors and cool colours over resistors (e.g. Figure 8). Alternatively, a 90 degree phase rotation (PR) is also applied to the grids of each tipper component. This transforms bipolar (i.e. cross-over) anomalies into single pole anomalies with a maximum over conductors, while preserving long wavelength information. The two orthogonal grids are then added together:

$$TPR = PR(T_{zx}) + PR(T_{zy}),$$

to obtain a total phase rotated (TPR) grid for each of the in-phase and quadrature components (e.g. Figure 9). In contrast to the cross-over behaviour demonstrated by ZTEM tipper data, the AirMt amplitude parameter display peak maxima and minima across conductive and resistive zones, respectively. Hence, no further processing of the AirMt data are required for plan-view presentation, as shown in the 75 Hz AP image in Figure 10.

300 Hz, and 600 Hz. Total magnetic intensity (TMI) data were also acquired using a caesium magnetometer for both surveys. Figure 7 shows the reduced-to-pole (RTP) magnetic response, which highlights a number of features, including: (a) a linear NS magnetic low over the Jameson fault, possibly due to alteration or overburden fill; (b) NE-trending magnetic lineaments, which mostly correlate with late mafic dolerite dykes; (c) a partial ring-like magnetic high centred on a magnetic low over the Babel deposit, that is likely responding to the increased sulphides on the outer perimeter of the intrusive; and (d) a broad magnetic high mainly centred with the Nebo intrusive that likely indicates increased magnetite content in the gabbro-norite body.

Examples of the 75 Hz ZTEM and AirMt data are shown in plan in Figures 8, 9 and 10. Multi-frequency profiles of the ZTEM and AirMt data are also presented in Figure 11, for a representative north-south flight line (L1430) across the Babel deposit. To present data from both tipper components in one

Comparing the three images in Figures 8 to 10, the ZTEM DT, TPR and AirMt AP results are remarkably consistent and highlight similar geologic features defined in the magnetic results, such as (a) the conductive Jameson fault that extends north and south of the survey area, (b) a ring-like conductive anomaly that partially coincides with the Babel deposit, and (c) a smaller conductive anomaly over the Nebo deposit that appears to coincide with the known massive sulphide lenses. Other ZTEM-AirMt conductive lineaments that are defined, in part, appear to correlate with either magnetic lineations or mapped faults, and may therefore indicate increased porosity or clay in the faults or possible near-surface paleochannel or
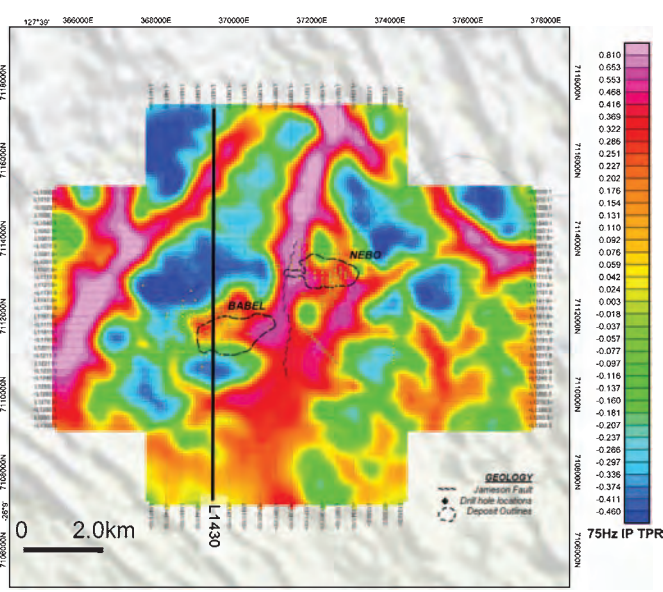

Fig. 9. *ZTEM 75Hz In-Phase Total Phase Rotation (TPR).*
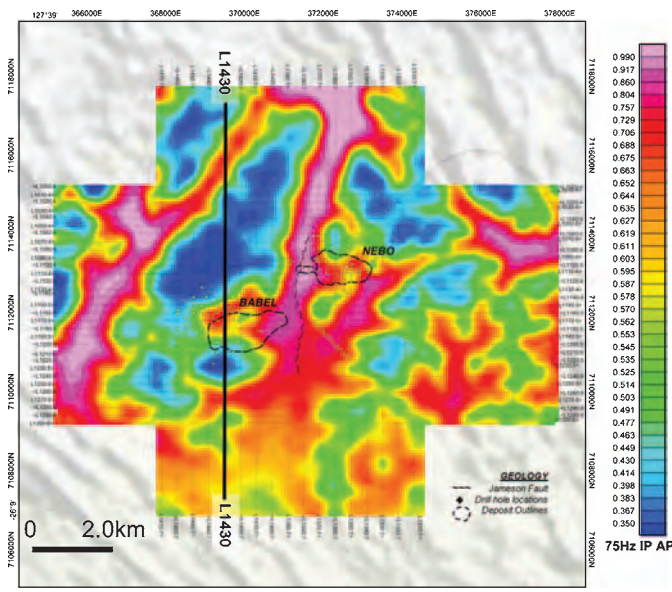

Fig. 10. *AirMt 75Hz In-Phase Amplitude Parameter (AP).*

overburden relief structures (G. Walker, pers. comm., 2011). What is clear from these results is that the cross-cutting behaviour in the ZTEM and AirMt clearly points to 3D geology. While the DT, TPR and AP grids can be used for qualitative analysis, neither they nor the data profiles themselves (Figure 11) are able to easily provide any quantitative information about these 3D structures. For this, 3D inversion is required.

2D inversion

Geotech's 2D inversion is based on modifications to the MT modelling algorithm of Wannamaker *et al.* (1987) with sensitivities by de Lugao and Wannamaker (1996) in an iterative Gauss-Newton method (Tarantola, 1987). The software is serial and runs on desktop computers. Each line is inverted independently. For 2D ZTEM inversion, this software only inverts the inline (T_{zx}) tipper data and assumes orthogonal and infinite strike length of all targets. For 2D AirMt inversion, the software inverts the amplification parameter assuming orthogonal and infinite strike length of all targets. This approximation is reasonable if the geological structures have strike lengths orthogonal to the flight line direction in the order of a skin depth; i.e. greater than the footprint or sensitivity of the ZTEM or AirMt systems. In both cases, the 2D ground topography and the air-layer thickness below the receiver are accounted for; however, the inversions also require *apriori* starting models that are reasonably close to the true half-space resistivity. At Nebo–Babel, 300 ohm-m was chosen for the starting half-space resistivity based on interpretations from a previous ground AMT survey provided by BHP Billiton.

For the Nebo–Babel 2D inversions, model convergence RMS fits of 1.0 or less were achieved in four to five iterations
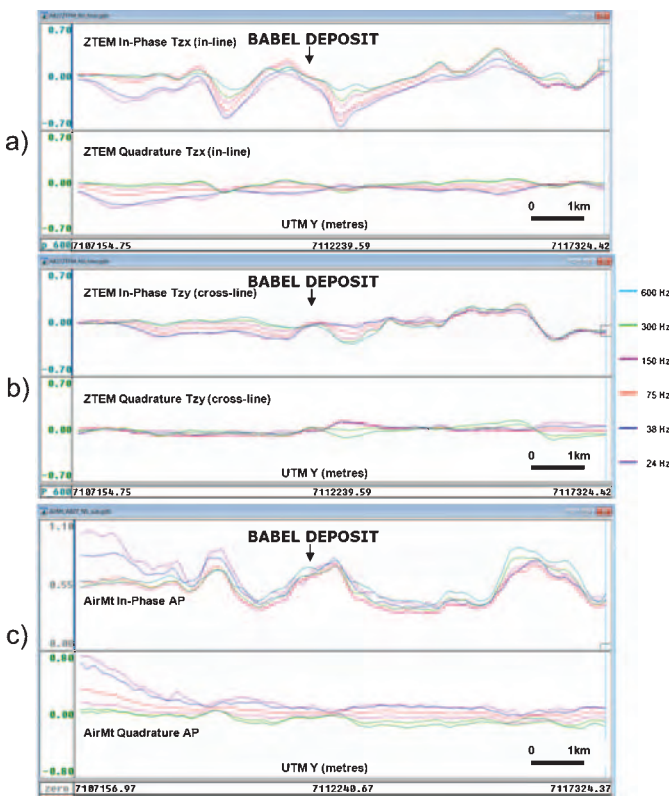
with data errors of 0.03–0.05 for ZTEM, whereas considerably higher data errors of 0.15–0.22 were required for AirMt. This relative inability to properly fit the data in 2D is interpreted to reflect the greater sensitivity of AirMt AP measurement to 3D distortion, relative to the ZTEM in-line component data, but also an indication the 3D geology at Nebo–Babel. Similarly, 2D inversions of data along north-south lines appear to best highlight the Nebo and Babel deposit responses, due to their dominant EW strike, with the ZTEM models seemingly more successful than AirMt. On the other hand, none of the technologies' 2D inversions along east-west lines (not shown) appear to successfully resolve either deposit clearly, due to the dominance of the Jameson Fault. Panels a) and b) of Figure 12 present 2D inversions of ZTEM and AirMt data, respectively, along the north-south L1430 profile, which crosses the Babel deposit – the approximate outline of the intrusion is also shown.

3D inversion

TechnoImaging's 3D modelling is based on the 3D integral equation method (Hursán and Zhdanov, 2002), and the inversion itself uses a regularised re-weighted conjugate gradient (RRCG) method with focusing stabilisers (Zhdanov, 2002). Unlike smooth regularisation, focusing enables the recovery of 3D models with higher contrasts and sharper boundaries. This is an analog of the 3D MT inversion described by Zhdanov *et al.* (2011). The software is fully parallelised for running on cluster computers, meaning that it can be scaled to invert very large survey areas. Panels c) and d) of Figure 12 show vertical cross-sections from the 3D inversions of ZTEM and AirMt data, respectively, along the L1430 north-south profile across the Babel deposit.

Comparing the 2D and 3D inversion cross-sections in Figure 12, at first glance, all four appear to show a reasonably well defined anomalous conductive response over the Babel deposit, with the maximum conductivity generally offset towards the north edge
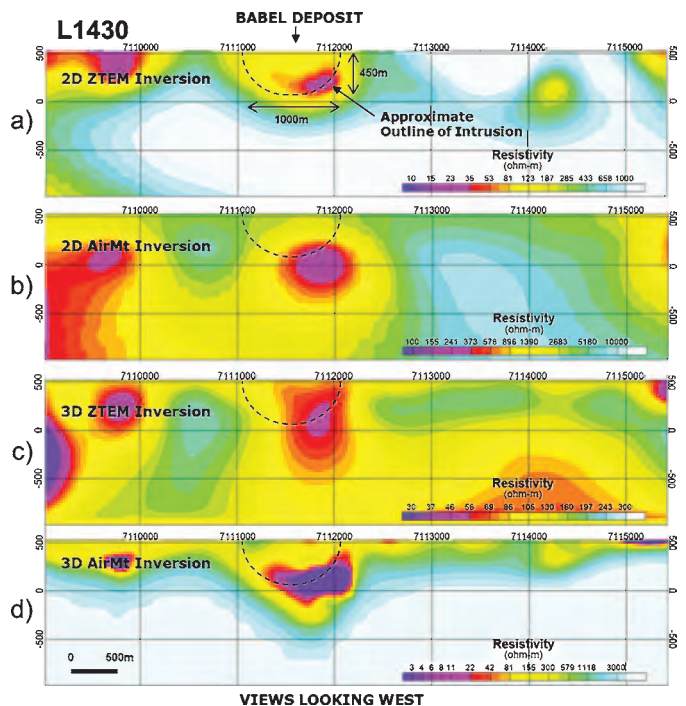

Fig. 11. *Multi-frequency (24–600 Hz) In-Phase and Quadrature data profiles for L1430 (a) ZTEM In-line (Tzx) component (XIP & XQD), (b) ZTEM Cross-line (Tzy) component (YIP & YQD), and (c) AirMt Amplitude Parameter (AIP & AQD).*

Fig. 12. *2D and 3D inversions along line L1430: (a) 2D ZTEM Inversion, (b) 2D AirMt inversion, (c) 3D ZTEM Inversion, and (d) 3D AirMt inversion.*

and base of the intrusive. Interestingly, this increased conductivity at depth is not easily supported geologically yet is a consistent feature in all four models. However, the overall shape and size extent of the semi-concentric intrusive appear to be better resolved in the 2D ZTEM and particularly in the 3D ZTEM and AirMt models, the lattermost that features the best resolved and most contrasted conductivity anomaly of the four. The generally lower resistivities found in the gabbro-norite are also consistent with ground AMT results (G. Walker, pers. comms, 2011). In contrast, the 2D AirMt model appears to overestimate the target depth, relative to the remaining three inversions, but this may also reflect the poorer quality model-misfits as well. The increased near-surface conductivity observed in all four model sections that extend south of Babel is consistent with heavier overburden cover – as also observed in ground AMT results.

Conclusions

Given global industry trends towards deeper exploration, ZTEM and AirMt represent practical airborne electromagnetic methods for mapping conductivity to depths in excess of 1 km. As natural source electromagnetic methods, ZTEM and AirMt are generated from robust data processing techniques that enable 3D quantitative interpretation. Interpretation of both ZTEM and AirMt data is analogous to magnetovariational (MV) data, and in principle similar to magnetotelluric (MT) data. In this paper, we have presented a review of the current acquisition and interpretation methodologies, including system descriptions, data processing and presentation, 2D inversion, and 3D inversion. We have demonstrated this with a case study involving the interpretation of over 500 line km of both ZTEM and AirMt data from BHP Billiton's Nebo–Babel Ni–Cu–PGE deposit in Western Australia's West Musgrave district.

Acknowledgements

References

Constable, S. C., Parker, R. L., and Constable, C. G. (1987). Occam's inversion: a practical algorithm for generating smooth models from EM sounding data. *Geophysics* **52**, 289–300.

de Lugao, P. P., and Wannamaker, P. E. (1996). Calculating the two-dimensional magnetotelluric Jacobian in finite elements using reciprocity. *Geophysical Journal International* **127**, 806–810. doi:10.1111/j.1365-246X.1996.tb04060.x

Farquharson, C. G., Oldenburg, D. W., Haber, E., and Shekhtman, R. (2002). An algorithm for the three-dimensional inversion of magnetotelluric data: *72nd Annual International Meeting, SEG, Expanded Abstracts*, 649–652.

Groves, D. I., Groves, I. M., Gardoll, S., Maier, W., and Bierlein, F. P. (2007). The West Musgrave – a potential world-class Ni-Cu-PGE sulphide and iron oxide Cu-Au province? Presented at AIG Conference, Perth.

Holtham, E., and Oldenburg, D. W. (2010). Three-dimensional inversion of ZTEM data. *Geophysical Journal International* **182**, 168–182.

Hursán, G., and Zhdanov, M. S. (2002). Contraction integral equation method in three-dimensional electromagnetic modeling. *Radio Science* **37**. doi:10.1029/2001RS002513.

Kaminski, V. F., Kuzmin, P., and Legault, J. M. (2010). AirMt – passive airborne EM system: Presented at 3rd CMOS-CGU Congress, Ottawa.

Kuzmin, P. V., Borel, G., Morrison, E. B., and Dodds, J. (2010). Geophysical prospecting using rotationally invariant parameters of natural electromagnetic fields: WIPO International Patent Application No. PCT/CA2009/001865.

Labson, V. F., Becker, A., Morrison, H. F., and Conti, U. (1985). Geophysical exploration with audiofrequency natural magnetic fields. *Geophysics* **50**, 656–664. doi:10.1190/1.1441940

Pare, P., and Legault, J. M. (2010). Ground IP-resistivity and airborne SPECTREM and helicopter ZTEM survey results over Pebble copper-moly-gold porphyry deposit, Alaska: *80th Annual International Meeting, SEG, Expanded Abstracts*, 1734–1738.

Sattel, D., Thomas, S., and Becken, M. (2010). An analysis of ZTEM data over the Mt Milligan porphyry copper deposit, British Columbia: *80th Annual International Meeting, SEG, Expanded Abstracts*, 1729–1733.

Seat, Z., Beresford, S. W., Grguric, B. A., Waugh, R. S., Hronsky, J. M. A., Gee, M. A. M., Groves, D. I., and Mathison, C. I. (2007). Architecture and emplacement of the Nebo-Babel gabbronorite-hosted magmatic Ni-Cu-PGE sulphide deposit, West Musgrave, Western Australia. *Mineralium Deposita* **42**, 551–581. doi:10.1007/s00126-007-0123-9

Seat, Z., Beresford, S. W., Grguric, B. A., Mary Gree, M. A., and Grassineau, N. V. (2009). Re-evaluation of the role of external sulfur addition in the genesis of Ni-Cu-PGE deposits – evidence from the Nebo-Babel Ni-Cu-PGE deposit, West Musgrave, Western Australia. *Economic Geology and the Bulletin of the Society of Economic Geologists* **104**, 521–538. doi:10.2113/gsecongeo.104.4.521

Tarantola, A. (1987). Inverse problem theory: Elsevier, Amsterdam.

Wannamaker, P. E., Stodt, J. A., and Rijo, L. (1987). A stable finite element solution for two-dimensional magnetotelluric modeling. *Geophysical Journal of the Royal Astronomical Society* **88**, 277–296. doi:10.1111/j.1365-246X.1987.tb01380.x

Ward, S. (1959). AFMAG – airborne and ground. *Geophysics* **24**, 761–787. doi:10.1190/1.1438657

Ward, S. H., O'Donnell, J., Rivera, R., Ware, G. H., and Fraser, D. C. (1966). AFMAG –applications and limitations. *Geophysics* **31**, 576–605. doi:10.1190/1.1439795

Zhdanov, M. S. (2002). Geophysical inverse theory and regularization problems: Elsevier, Amsterdam.

Zhdanov, M. S., Smith, R. B., Gribenko, A., Čuma, M., and Green, A. M. (2011). Three-dimensional inversion of large-scale EarthScope magnetotelluric data based on the integral equation method – geoelectrical imaging of the Yellowstone conductive mantle plume. *Geophysical Research Letters* **37**. 10.1029/2011GL046953.